Wavefront Reconstruction Using Intensity Measurements for Real-time Adaptive Optics

João Silva[1], Elisabeth Brunner[1], Alessandro Polo[2], Cornelis de Visser[3], Michel Verhaegen[1]

***Abstract*— The crucial step in Adaptive Optics feedback control is the reconstruction of the wavefront. For a classical real-time feedback control a (Shack-)Hartmann wavefront sensor is used and that makes the wavefront reconstruction problem linear. In this paper a new methodology is proposed to reconstruct the wavefront for real-time AO control using the complete intensity measurement provided by the sensor and not just their centroids. In addition to an outline of the new wavefront reconstruction method, its performance is illustrated via a numerical simulation study. The advantages of the new method are highlighted by (a) integrating the method in a classical AO feedback loop and (b) comparing the new wavefront reconstruction method in a simulation study with the classical centroid algorithm based wavefront reconstruction in real-time classical AO feedback control.**

I. Introduction

High resolution imaging with for example telescopes, microscopes or lithography machines is often hampered by the presence of aberrations in the wavefront. Such aberrations are induced in various ways. For example in astronomical observations with ground based telescopes, the aberrations are due to atmospheric turbulence, temperature gradients, etc. Adaptive Optics (AO) was proposed more then half a century ago [1], but is now more and more being used to correct these aberrations in real-time. An AO system consists of a sensor measuring information from which the wavefront aberrations can be reconstructed and an actuator to correct these aberrations. For classical real-time AO control where the bandwith of the feedback controller is far off the first resonance frequency of the deformable mirror, used as an actuator, the key problem is the reconstruction of the wavefront. For that purpose, a (Shack-) Hartmann wavefront sensor is the preferred device since it enables the formulation of the wavefront reconstruction problem as a linear (least squares) problem.

In this paper we restrict ourselves to the Hartmann wavefront sensor for simplicity and brevity although the results are extendable to the Shack-Hartmann architecture. The Hartmann wavefront sensor consists of an array of apertures that sample the incoming wavefront. The centroid algorithm then provides an *approximation* of the spatial slope of the wavefront for each aperture. This algorithm computes the center of mass of the intensity measurements collected by a detector (e.g. CCD camera) thus losing some of the information present in the intensity patterns. This will in general cause a loss in accuracy of the wavefront reconstruction results.

In order to preserve the main advantage of the centroid based wavefront reconstruction, that is the *linearity* of the wavefront reconstruction problem, but to make direct use of the measured intensities as in [2] without first approximating the spatial slopes, a new wavefront reconstruction method is presented in this paper. The method is based on the integration of two principles. The first is a physical principle where we perform a distributed linearization of the relationship between the local wavefront aberrations and the intensity measurements of the aperture that "sees" this local wavefront. The second is a numerical principle on the use of B-splines to parametrize and reconstruct the unknown wavefront. The methodology of parametrizing the wavefront in the B-spline wavefront is based on our recent work in [3], [4] .

The paper is organized as follows. The new method is described in Section III. A simulation study of the new wavefront reconstruction method is presented in Section IV. Here a comparison is made with the classical modal reconstruction method [5] which uses slope measurements provided by the centroid algorithm [6]. The comparison is made in an open-loop and closed-loop configuration. For the classical AO feedback control it will be assumed that the deformable mirror is perfect and that the wavefront aberration is static. Such a classical AO control methodology described in a control engineering framework is e.g. given in [7], [8]. Finally we end this paper with some concluding remarks.

II. The Adaptive Optics Control Problem

To explain the principle of AO, and the role of wavefront reconstruction in the closed loop, we will briefly outline an AO application in an astronomical context. For that purpose consider the schematic drawing in Figure 1. When light from a distant star arrives at the outer layers of the atmosphere, it has a perfectly plane wavefront. However, this plane wavefront will reach the telescope deformed as the turbulent atmosphere will introduce time and space varying optical path length differences. This gives rise to a turbulence induced phase profile $\phi(r,t)$, where $r \in \mathbb{R}^2$ specifies the spatial position in the telescope aperture and t denotes time. The AO system tries to cancel out these wavefront distortions by actively introducing optical path length differences of opposite sign.

[1]These authors are with the Delft Center for Systems and Control, Faculty of Mechanical, Maritime, and Materials Engineering, Delft University of Technology, Delft 2628 CD, The Netherlands. Corresponding author: j.p.lopesesilva@student.tudelft.nl

[2]Alessandro Polo is with the Optics Research Group, Delft University of Technology, Lorentzweg 1, 2628 CJ Delft, The Netherlands

[3]Cornelis de Visser is with the Control and Simulation Division, Faculty of Aerospace Engineering, Delft University of Technology, 2600GB Delft, The Netherlands

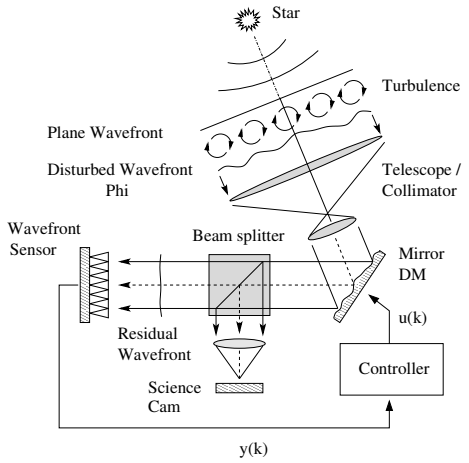

Fig. 1: Schematic representation of an AO system, and its main components.

An AO system is typically composed of the following components – a wavefront sensor (WFS), a wavefront corrector element to influence the phase and a feedback controller. In most systems, like the one depicted in Figure 1, the wavefront corrector element is a deformable mirror (DM). For the ease of discussion we will simply assume that the active component is a DM.

Light that "enters" the AO system is first directed to the DM. By changing the mirror shape in real-time, the DM is able to apply a time-varying phase correction $\phi_{dm}(r,t)$. The residual phase error is the difference between the turbulence induced wavefront and the applied correction, i.e. $\epsilon = \phi - \phi_{dm}$. After applying the wavefront correction, a beam splitter divides the reflected light beam in two parts. The first part of the corrected light beam leaves the AO system and is used by the science camera for object image formation. The remaining light is directed to the WFS, which provides quantitative information about the residual wavefront. Based on the WFS measurements $s(\cdot)$, the controller has to determine the actuator inputs $u(\cdot)$ to the DM. The controller should adapt the input signal in such a way that the DM cancels out most of the distortions. The latter degree of compensation is specified in terms of control criteria, like the so-called H_2 criterium [8].

By counteracting the wavefront distortions, AO is able to reduce the degrading effect of atmospheric turbulence on the imaging process. The goal of an AO system is to keep the wavefront of the light reaching the science camera to be as flat as possible. In this way, the corrected image can be recorded without being spread out when using long exposure times. By using AO, large ground-based based telescopes may reach close to diffraction limited performance in the near infrared [9], [10].

III. Wavefront Reconstruction

In this paper we consider the AO configuration as depicted in Figure 1. For a wavefront sensor, we consider a Hartmann array. This Hartmann Wavefront Sensor (HWS) consists of an array of apertures equally spaced in an otherwise opaque screen. The wavefront is sampled by each subaperture at the aperture plane and the transmitted beams are collected by a detector, like a CCD camera [2]. The classical approach uses the recorded intensities behind each aperture to extract an approximation of the local spatial gradient of the wavefront. In this paper the novel idea is to propose the use of all recorded intensity measurements in the wavefront reconstruction. In the following subsection we derive the model that is used for relationship between the wavefront and the intensity measurements, its local linearization, modeling of the wavefront via B-splines and constrained least squares solution. In the scope of this brief paper, we restrict to presenting only a centralized solution. But following our work in [11] this method has the potential to be distributed and hence to become useful for large scale AO.

A. General intensity-based phase retrieval algorithm

The complex field of the wavefront immediately after being transmitted by the Hartmann hole array can be described by its amplitude $A(x,y)$ and its phase distribution $\Phi(x,y)$. The complex field $U(x,y,z)$ can then be defined in the aperture plane ($z=0$) and detector plane ($z=L$) as follows:

$$U(x,y,0) = A(x,y)\exp(i\nu\Phi(x,y)) \tag{1}$$

$$U(x,y,L) = \mathscr{F}^{-1}\left[\mathscr{F}[U(x,y,0)]H(f_x,f_y)\right] \tag{2}$$

where $H(f_x,f_y)$ represents the Rayleigh-Sommerfield transfer function [12] (which depends on the spatial frequencies f_x and f_y) and ν represents the wavenumber.

The phase Φ can be parametrized as a linear combination of K general basis functions f_k.

$$\Phi(x,y) = \sum_{k=1}^{K} \alpha_k f_k(x,y) \tag{3}$$

These coefficients α_k can be estimated by minimizing the error between the intensity of the field given by the model and the measured intensity. Let $F(x_i,y_j)$ represent the measured intensities of each pixel (i,j) at the detection plane and let $I(x_i,y_j,L) = |U(x_i,y_j,L)|^2$ be the intensity given by the physical model also evaluated in pixel (i,j). With these two quantities one is able to define a simple cost function (Eq. (4)). For the sake of simplicity, the plane defined by the variables (x,y) will be sampled in such a way that (x_i,y_j) correspond to the center of the pixel (i,j).

$$J = \sum_{i,j} \left[F(x_i,y_j) - I(x_i,y_j,L)\right]^2 \tag{4}$$

In [2] a nonlinear least squares optimization procedure was performed to estimate the coefficients α_k that describe the phase distribution (3). However, as presented in the next section, a linearisation can be made to simplify the problem.

B. Formulation of the linearised problem

Firstly, both $F(x_i, y_j)$ and $I(x_i, y_j, L)$ in (4) are vectorized such that, given a total of M pixels, two vectors $\mathbf{f}$ and $\mathbf{i_L} \in \mathbb{R}^{M\times 1}$ are created. Thus, a new cost function J_{vec} can then be defined.

$$J_{\text{vec}} = ||\mathbf{f} - \mathbf{i_L}||_2^2 \tag{5}$$

$$= \sum_{m=1}^{M} \left(F(m) - I(m, L)\right)^2 \tag{6}$$

Note that each element m of the newly created vectors has a direct mapping to a point (x_i, y_j) in the Cartesian plane.

In order to find the coefficients that minimize J_{vec} using a linear method, we linearise the intensity term defined at a certain pixel $I_L(m) = I(m, L)$ using a first-order Taylor series around an arbitrary vector of phase coefficients $\tilde{\boldsymbol{\alpha}}$. In this case we will use $\tilde{\boldsymbol{\alpha}} = 0$.

$$I_L(m) = U_L^*(m)U_L(m) \tag{7}$$

$$\frac{\partial I_L(m)}{\partial \boldsymbol{\alpha}} = \left[\frac{\partial U_L^*(m)}{\partial \boldsymbol{\alpha}} U_L(m) + U_L^*(m)\left(\frac{\partial U_L(m)}{\partial \boldsymbol{\alpha}}\right)\right] \tag{8}$$

The truncated first-order Taylor can then be expressed as follows:

$$\begin{aligned} I_L(m) &\approx I_L(m)_{\boldsymbol{\alpha}=\tilde{\boldsymbol{\alpha}}} + \left[\frac{\partial U_L^*(m)}{\partial \boldsymbol{\alpha}} U_L(m) + \right. \\ &\left. + U_L^*(m)\,\frac{\partial U_L}{\partial \boldsymbol{\alpha}}(m)\right]_{\boldsymbol{\alpha}=\tilde{\boldsymbol{\alpha}}} \boldsymbol{\alpha} \\ &= c_{0m} + c_{1m}\boldsymbol{\alpha} \end{aligned} \tag{9}$$

where

$$\frac{\partial U_L(m)}{\partial \boldsymbol{\alpha}} = \begin{bmatrix} \frac{\partial U_L(m)}{\partial \alpha_1} & \cdots & \frac{\partial U_L(m)}{\partial \alpha_K} \end{bmatrix} \in \mathbb{R}^{1\times K}$$

$$\frac{\partial U_L(m)}{\partial \alpha_k} = \mathscr{F}^{-1}\left[\mathscr{F}[U_0(m) i\nu f_k(m)] H(m)\right] \tag{10}$$

Notice that the index m pertaining to the transfer function $H(m)$ does not refer to a mapping between a given pixel and a point in the Cartesian plane but to a point in the spatial frequencies domain. The details about the implementation can be found in [13].

The terms c_{0m} and c_{1m} in Eq. (9) are computed for each $m = 1, ..., M$ in order to define $\mathbf{c_0} = [c_{01}, ..., c_{0M}]^T \in \mathbb{R}^{M\times 1}$ and $\mathbf{C_1} = [c_{11}, ..., c_{1M}]^T \in \mathbb{R}^{M\times K}$. This new formulation is helpful in order to present the new cost function J_{lin} for the linearized problem:

$$J_{\text{lin}} = ||\mathbf{f} - (\mathbf{c_0} + \mathbf{C_1}\boldsymbol{\alpha})||_2^2 \tag{11}$$

The optimal solution for this problem is then:

$$\hat{\boldsymbol{\alpha}} = (\mathbf{C_1}^T\mathbf{C_1})^{-1}\mathbf{C_1}^T(\mathbf{c_0} - \mathbf{f}) \tag{12}$$

The final step needed to present the algorithm is to present the spline framework which is done in the next section.

C. Multivariate simplex B-splines

The nomenclature used to define these basis functions will follow closely the one presented in [4], [3].

To provide a brief summary regarding the way these basis functions are created an initial clarification regarding all the terminology used is necessary. The splines used in this application are multivariate as they are defined in a simplex in a 2 dimensional space. A simplex is, in the 2-D case, a triangle which means that it can be defined by 3 non-degenerate vertices $(\mathbf{v_0}, \mathbf{v_1}, \mathbf{v_2}) \in \mathbb{R}^{2\times 3}$. Furthermore, to evaluate the value of the spline efficiently we use the barycentric coordinate system.

Given a certain point $\mathbf{x} = (x, y)$ belonging to the Cartesian plane a barycentric coordinate in $\mathbb{R}^3$ can be determined as follows:

$$\begin{bmatrix} b_1 \\ b_2 \end{bmatrix} = \mathbf{V}^{-1}\begin{bmatrix} x \\ y \end{bmatrix} \tag{13}$$

$$b_0 = 1 - b_1 - b_2 \tag{14}$$

where the transformation matrix $\mathbf{V}$ can be defined as

$$\mathbf{V} = \begin{bmatrix} \mathbf{v_1} - \mathbf{v_0} & \mathbf{v_2} - \mathbf{v_0} \end{bmatrix} \tag{15}$$

Using the barycentric coordinates, the following equations completely define the basis functions B_κ^d of a certain degree d defined in a certain simplex t. This simplex belongs to a more general partition of the domain in non-overlapping simplices, a triangulation, represented by $\mathcal{T}$.

$$(b_0 + b_1 + b_2)^d = \sum_{\kappa_0+\kappa_1+\kappa_2} \frac{d!}{\kappa_0!\kappa_1!\kappa_2!} b_0^{\kappa_0} b_1^{\kappa_1} b_2^{\kappa_2} \tag{16}$$

where $|\kappa| = \kappa_0 + \kappa_1 + \kappa_2 = d$ and $\kappa_0, \kappa_1, \kappa_2 \geq 0$

$$B_\kappa^d(b(\mathbf{x})) = \begin{cases} \frac{d!}{\kappa_0!\kappa_1!\kappa_2!} b_0^{\kappa_0} b_1^{\kappa_1} b_2^{\kappa_2} & , \mathbf{x} \in t \\ 0 & , \mathbf{x} \notin t \end{cases} \tag{17}$$

Weighting the basis functions yields a B-form polynomial $p(b(\mathbf{x}))$ of the form

$$p(b(\mathbf{x})) = \begin{cases} \sum_{|\kappa|=d} \alpha_\kappa^t B_\kappa^d & , \mathbf{x} \in t \\ 0 & , \mathbf{x} \notin t \end{cases} \tag{18}$$

One of the main advantages of using B-splines is the fact one can force continuity of order r such that all m-th order derivatives, with $0 \leq m \leq r$, of two B-form polynomials defined on two neighbouring simplices are equal on the edge between the simplices.

In [3], a general method was created to guarantee continuity between all the common edges of neighbouring B-form polynomials. The method yields a smoothness matrix $\mathbf{H}$ that establishes a relationship between the coefficients of the neighbouring polynomials:

$$\mathbf{H}\boldsymbol{\alpha} = 0 \tag{19}$$

After this brief explanation concerning the B-splines, all the fundamental concepts and definitions necessary to solve the problem in Eq. (11) are now presented which leads us to introduce the local optimization problem for a single subaperture.

D. Subaperture local problem

In this phase retrieval method, we propose that both the aperture and detection plane are divided in N (where N is the number of subapertures) equal and adjacent square regions each of them encompassing the entire subaperture and the corresponding square space (subimage) in the detection plane. We will use the data from the subimage on the detection plane to estimate the phase only in its corresponding subaperture.

Provided that the diffraction effects on the detection plane are small, one can guarantee that the propagated beams from one subaperture have a minimal effect in the subimage corresponding to another subaperture. Therefore, the linear optimization procedure defined in (11) can be applied locally and almost independently to estimate the phase distribution in each of the subapertures.

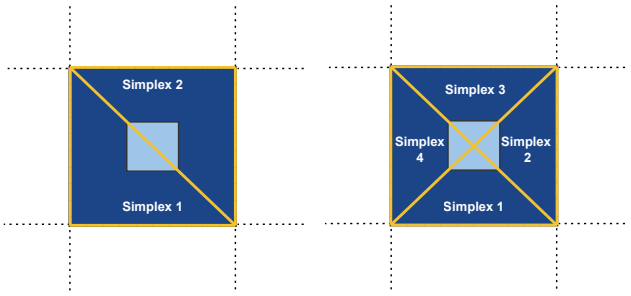

Fig. 2: Close-up on one of the subapertures. In the left (right) subaperture a type I (II) triangulation was defined using 2 (4) simplices per subaperture

The local areas that have been defined in both planes are square whereas the B-splines are defined in a simplex with a triangular shape. Therefore, the phase distribution was parametrized using J triangles that divide the subaperture. An example with 2 (type I triangulation) and 4 (type II triangulation) can be seen in Figure 2.

In order to ensure continuity in the same subaperture one may enforce the continuity constraints (Eq. (19)) inherent to the spline framework. The word may is used as these constraints are not nearly as important as the ones that connect the different subapertures which will be presented in the next section. The formulation of the local problem is presented in (20) for a certain aperture n.

$$\begin{aligned} &\min \left\| \begin{bmatrix} \mathbf{f}_1^n \\ \vdots \\ \mathbf{f}_J^n \end{bmatrix} - \begin{bmatrix} \mathbf{c}_{0,1}^n \\ \vdots \\ \mathbf{c}_{0,J}^n \end{bmatrix} - \begin{bmatrix} \mathbf{C}_{1,11}^n & \cdots & \mathbf{C}_{1,1J}^n \\ \vdots & \ddots & \vdots \\ \mathbf{C}_{1,J1}^n & \cdots & \mathbf{C}_{1,JJ}^n \end{bmatrix} \begin{bmatrix} \boldsymbol{\alpha}_1^n \\ \vdots \\ \boldsymbol{\alpha}_J^n \end{bmatrix} \right\|_2^2 \\ &\text{s.t.} \quad \mathbf{H}^{\text{local}} \begin{bmatrix} \boldsymbol{\alpha}_1^n \\ \vdots \\ \boldsymbol{\alpha}_J^n \end{bmatrix} = 0 \end{aligned} \tag{20}$$

E. Global optimization

The natural extension to Eq. (20) is to perform this optimization for all the subapertures simultaneously. For the optimization to be successful it is not enough to purely replicate the procedure presented in Eq. (11). Additional boundary constraints must be inserted in addition to those that provide continuity between the two neighbouring polynomials in each of the subapertures.

Let us provide an example. Take, for instance, the upper simplex in the left subaperture in Figure 2. Assuming that the adjacent subapertures have the same simplex layout, continuity constraints should be imposed to connect the aforementioned simplex with the lower simplices of the subapertures which are located upwards and to the right. These constraints should also be included in the smoothness matrix $\mathbf{H}$ so as to generate a global problem for N subapertures.

$$\begin{aligned} &\min \left\| \begin{bmatrix} \mathbf{f}^1 \\ \vdots \\ \mathbf{f}^N \end{bmatrix} - \left(\begin{bmatrix} \mathbf{c}_0^1 \\ \vdots \\ \mathbf{c}_0^N \end{bmatrix} + \mathbf{C}_1^{\text{global}} \begin{bmatrix} \boldsymbol{\alpha}^1 \\ \vdots \\ \boldsymbol{\alpha}^N \end{bmatrix} \right) \right\|_2^2 \\ &\text{s.t.} \quad \mathbf{H}^{\text{global}} \begin{bmatrix} \boldsymbol{\alpha}^1 \\ \vdots \\ \boldsymbol{\alpha}^N \end{bmatrix} = 0 \end{aligned} \tag{21}$$

where,

$$\mathbf{C}_1^{\text{global}} = \begin{bmatrix} \mathbf{C}_1^1 & & \\ & \ddots & \\ & & \mathbf{C}_1^N \end{bmatrix}$$

The solution for this problem can be found in an iterative or direct way as described in [3].

IV. Simulation Results

A. Demonstration of Operation of the new method

In this section, the performance of our our method is compared against a modal wavefront reconstruction algorithm presented in [5]. In the latter method, the wavefront is parametrized using Zernike basis functions and their weighting coefficients are estimated (using a least-squares approach) by fitting the slope measurements to the derivative of the previously parametrized wavefront. The centroid algorithm used to compute the slope measurements is presented in [6].

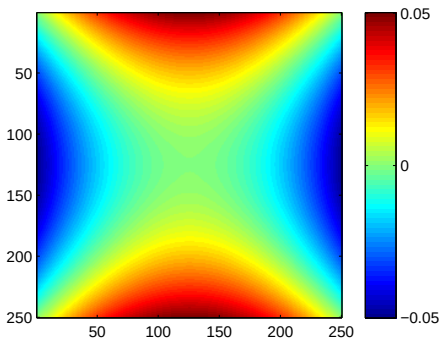

(a)

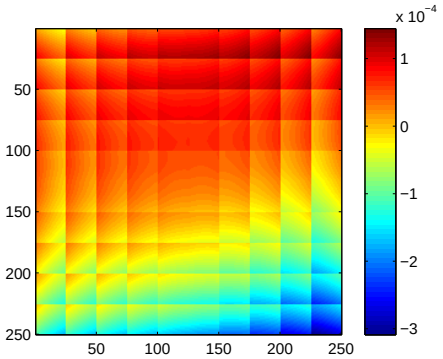

(b)

Fig. 3: (a) Reconstructed phase distribution for $\alpha_4 = 0.1\lambda$ and (b) its error (both normalized to the wavelength λ) when the intensity distribution was subject to noise ($\sigma = 4\times10^{-4}$)

The setup simulated is similar to the one presented in [2]. Each hole has a side length of 200 μm and is separated from the adjacent hole by a distance of 562.5 μm. The propagation distance (i.e., the distance between the aperture plane and the detection plane) is 10 mm and the wavelength is $\lambda = 638$nm. A grid of 10 by 10 subapertures was used to obtain these results.

White noise is can be modelled using a zero-mean Gaussian distribution with a certain standard deviation σ. In this setup the noise was added to the normalized intensity measures (with values between 0 and 1) and had a standard deviation of $\sigma_{\text{ccd}} = 4 \times 10^{-4}$ based on the specifications of a commercial camera.

A 4th order Zernike mode (according to Noll notation [14]) was used to model the incoming wavefront. The polynomial functions of the B-splines were chosen to have a degree $d = 2$ and subject to continuity constraints of order $r = 2$. A type II triangulation partitions the subapertures as per Figure 2.

The results presented in Figure 4 show that our method yields an RMS error approximately 1 order of magnitude lower in relation to the modal reconstruction method in the presence of noise for aberrations smaller than λ. In the noiseless case and for aberrations smaller than 0.1λ this method is able to provide an improvement of 2 orders of magnitude. For aberrations larger than 10λ, the diffraction pattern pertaining to a subaperture will affect the intensity pattern originating from other subapertures. In that case, our locality assumption is not verified and the method does not yield good results. It performs even poorer than the modal reconstruction for $\alpha_4 \geq 100\lambda$.

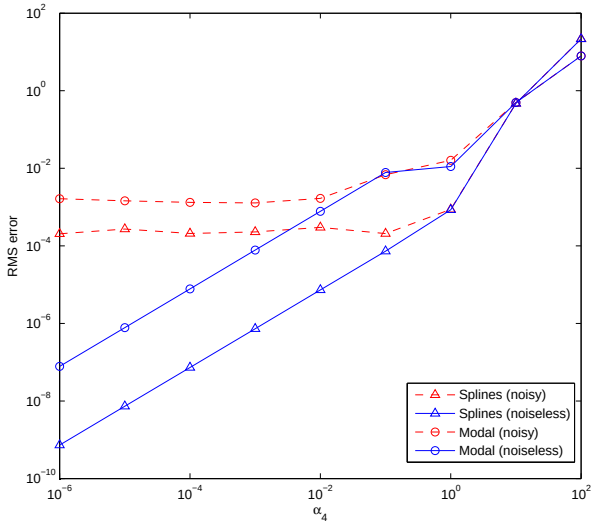

Fig. 4: Comparison of the RMS of the wavefront reconstruction between the new spline based WFR method and the modal reconstruction method (in open-loop). It is clear that due to the influence of the noisy measurements the RMS values reach a threshold when the aberrations get smaller: around $1.5\times10^{-3}\lambda$ for modal reconstruction and $2.5\times10^{-4}\lambda$ for spline-based reconstruction. Other experiments were done with different incoming wavefronts and the results were similar to the one presented above.

For incoming wavefronts modelled using high frequency Zernike modes the method presents results with the same accuracy as presented in Figure 4 provided that the degree of the spline functions is increased. That is due to the fact that the Zernike basis functions have a polynomial term in terms of the radius. The degree of that term is called the radial degree and in order to approximate it correctly the splines polynomials must have at least the same degree. For example, if we wanted to approximate Zernike modes accurately from the 7th until the 10th (radial degree equals 3) we would have to choose at least a spline degree $d = 3$. To filter out the noise the continuity constraints should be of the same order, that is, $r = 3$.

B. Closed loop comparison

So far, the results presented only concerned the open-loop reconstruction where no feedback loop nor deformable mirror is included. In this section, the methods used previously for wavefront reconstruction were integrated in a classical AO feedback loop (Figure 5) in order to analyse the convergence properties and sensitivity to noise of the wavefront reconstruction error.

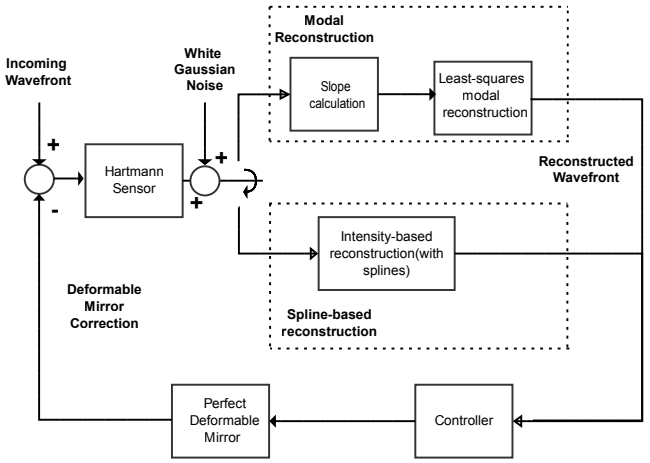

Fig. 5: Simplified representation of a feedback loop used in Adaptive Optics

The closed-loop setup includes the Hartmann sensor and the reconstruction algorithm with the same characteristics specified in Sec. IV-A. It also includes the deformable mirror, which in this case is assumed to be perfect, meaning that it will take the exact shape of the reconstructed wavefront. Furthermore, a delay was added in the loop simulating the time consumed by the computations and communications in a real-time implementation. To counteract the effect of the delay a PI controller was also integrated and tuned in order to minimize the effect of the delay.

Using a wavefront characterized by an astigmatism aberration with a coefficient of 0.1λ we obtain the results presented in Figure 6.

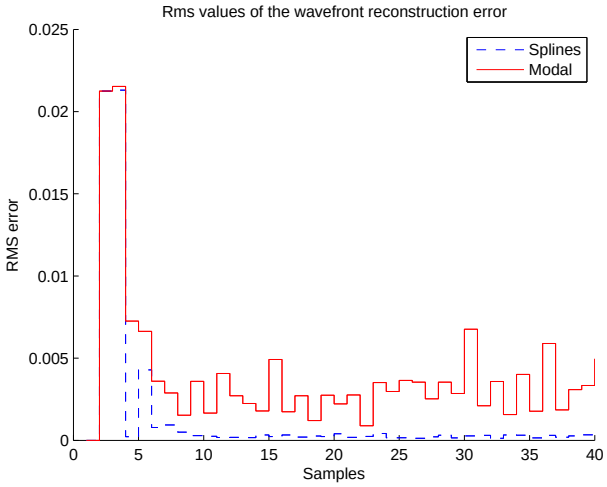

Fig. 6: RMS error evolution for a classical AO setup comparing the modal and the spline-based reconstruction method.

With this approach the reconstruction error converges to a lower RMS value and is less sensitive to noise than the closed loop with modal reconstruction.In the presence of noise the modal reconstruction method can not achieve the threshold for small aberrations in open-loop that is visible in Figure 4 while our method can.

V. Conclusions

With this method a successful replacement for the classical slope measurement phase retrieval techniques is presented. This linear method provides an improvement of approximately one order of magnitude in terms of RMS error regarding the classical methods for aberrations smaller than λ. Besides that it is capable of approximating high frequency Zernike with the same accuracy as presented in Figure 4 for the low frequency mode, provided that the degree of the approximating splines is chosen to match that of the radial degree of the Zernike mode. Moreover, given the structure of the Hartmann sensor the problem has the potential to be solved in a distributed way.

In an AO control perspective this method can be easily implemented in real-time feedback setups given its linearity. Besides that, integrating this novel method in a classical AO feedback loop will yield a lower reconstruction error in all the cases mentioned in the previous paragraph provided that the deformable mirror has sufficient resolution to depict accurately the reconstructed phase.

This method can be also applied to a phase reconstruction using intensity measurements from a Shack-Hartmann wavefront sensor.

References

[1] H. W. Babcock, "The possibility of compensating astronomical seeing," *Publications of the Astronomical Society of the Pacific*, vol. 65, no. 386, pp. 229–236, Oct. 1953.

[2] A. Polo, V. Kutchoukov, F. Bociort, S. Pereira, and H. Urbach, "Determination of wavefront structure for a Hartmann Wavefront Sensor using a phase-retrieval method," *Optics Express*, pp. 7822–7832, 2012.

[3] C. Visser, *Global Nonlinear Model Identification with Multivariate Splines*, 2012.

[4] C. Visser and M. Verhaegen, "Wavefront reconstruction in adaptive optics systems using nonlinear multivariate splines," *Journal of the Optical Society of America A*, vol. 30, no. 1, pp. 8295–8301, 2013.

[5] W. H. Southwell, "Wavefront estimation from wavefront slope measurements," *J. Opt. Soc. Am.*, vol. 70, no. 8, pp. 998–1006, Aug 1980.

[6] L. A. Carvalho, "A simple and effective algorithm for detection of arbitrary Hartmann–Shack patterns," *Journal of Biomedical Informatics*, vol. 37, no. 1, pp. 1 – 9, 2004.

[7] K. Hinnen, M. Verhaegen, and N. Doelman, "Exploiting the spatio-temporal correlation in adaptive optics using data driven h_2-optimal control," *Journal of the Optical Society of America A*, vol. 24, no. 5, pp. 1714–1725, 2007.

[8] ——, "A data driven H2-optimal control approach for adaptive optics," *IEEE Trans. on Control Systems Technology*, vol. 16, no. 3, pp. 381–395, 2008.

[9] G. Rousset, J. C. Fontanella, P. Kern, and F. Rigaut, "First diffraction-limited astronomical images with adaptive optics," *Astronomy and Astrophysics*, vol. 230, no. 2, pp. L29–L32, Apr. 1990.

[10] J. M. Beckers, "Adaptive optics for astronomy: Principles, performance, and application," *Annual review of astronomy and astrophysics*, vol. 31, pp. 13–62, 1993.

[11] *A Distributed simplex B-splines based Wavefront Reconstruction*, 2012.

[12] J. Goodman, *Introduction to Fourier Optics*. Roberts and Cia. Publ., 2005.

[13] D. Voelz, *Computational Fourier Optics*. SPIE Press, 2011.

[14] D. Malacara and W. T. Welford, *Optical shop testing*. John Wiley Sons, Inc., 2006.